Danish Meteorological Institute
Ministry for Energy, Utilities and Climate

DMI Report 17-16

Construction of a cloud burst index in numerical weather prediction

Niels Woetmann Nielsen, Bjarne Amstrup and Claus Petersen

Colophone Serial title:
DMI Report 17-16

Title:
Construction of a cloud burst index in numerical weather prediction

Subtitle:

Authors:
Niels Woetmann Nielsen, Bjarne Amstrup and Claus Petersen

Other Contributers:

Responsible Institution:
Danish Meteorological Institute

Language:
English

Keywords:
cloud burst, cloud burst index, indicator, CIN, CAPE, vertical integrated water vapour, vertical integrated water vapour at saturation, steering level wind, thunderstorm index

Url:
www.dmi.dk/laer-om/dmi-publikationer/2013/17-16

ISSN:
2445-9127

ISBN:
978-87-7478-670-2

Version:
1

Link til hjemmeside:
www.dmi.dk/laer-om/dmi-publikationer/2013

Dansk Resume

Der foreslås otte varianter af et skybruds-indeks (I_{cb}). De er alle vægtede produkter af et antal indikatorer. Hver indikator repræsenterer en egenskab ved troposfæren, som har indflydelse på skybrudsgenererende dyb fugtig konvektion. Alle indikatorer har værdier mellem 0 og 1, og ændrer brat værdi fra nær 0 til nær 1 ved en specificeret tærskelværdi, som har indikatorværdi 0.5. Vertikal integreret vanddamp, vertikal integreret vanddamp ved mætning, styringsvind, konvektiv inhibition og konvektiv tilgængelig potentiel energi er blandt indikatorerne. Flere 'case' studier præsenteres. I alle, undtagen et 'case', er der observeret mindst et skybrud i Danmark. I 'caset' uden registrerede skybrud var den forudsagte I_{cb} lille. I alle de andre 'case' studier var den forudsagte I_{cb} stor (0.8 til 1) på lokaliteter, hvor der blev registreret skybrud. Der var også områder med store I_{cb} værdier, hvor der ikke blev rapporteret skybrud. Dette indikerer en relativ høj falsk alarm rate, som er relateret til skybruds lave forudsigelighed. 'Case' studierne indikerer at I_{cb} er værdifuld, først og fremmest ved at udpege områder med høj risiko for skybrud. I ingen af 'case' studierne blev der rapporteret skybrud i områder med små værdier af I_{cb}.

Abstract

Eight variants of a cloud burst index, I_{cb}, are proposed. They are all weighted products of a number of indicators. Each indicator represents a property of the troposphere important for cloud burst generating deep moist convection. All indicators have values between 0 and 1, and shift rather abruptly from near 0 to near 1 at specified tresholds with indicator values equal to 0.5. Vertical integrated water vapour, vertical integrated water vapour at saturation, steering level wind speed, convective inhibition and convective available potential energy are among the indicators. Several case studies are presented. In all, except one, of these studies one or more cloud bursts were reported in Denmark. In the case with no cloud burst observations the predicted I_{cb} was low. In all the other cases the predicted I_{cb} was high (0.8 to 1) at locations where cloud bursts had been reported. There were also areas with high I_{cb} without reports of cloud bursts, indicating a relatively high false alarm rate, which to a large extend can be associated with the low predictability of cloud bursts. The case studies seem to show that I_{cb} is valuable in the sense that it points to high risk areas that overlap locations with reported cloud bursts. Stated in another way: In none of the case studies cloud bursts were recorded outside the high risk I_{cb} areas.

1 Introduction

Prediction of cloud bursts/flash-floods is a challenge, not only several hours to a day or more ahead, but also in the first few hours. Whether or not such systems develop usually depend on a number of meteorological parameters exceeding simultaneously certain thresholds. Several instability indices have been proposed as measures of the probability of convection and its severity (e.g. Bluestein, 1993). These indices account for some, but not all, of the parameters important for development of cloud bursts/flash-floods.

In the present report the idea is to construct a more general index, also accounting for parameters such as vertically integrated water vapour, vertically integrated water vapour at saturation and the steering level wind for Deep Moist Convection (DMC) cells. The added parameters are known to be important for development of cloud bursts/flash-floods.

The methodology used in the construction of the cloud burst/flash-flood index, I_{cb}, is described in Section 2, the indicators used in I_{cb} are defined in Section 3, and Section 4 presents the definition of I_{cb}. In Section 5 index values I_{cb} for Schleswig (Northern Germany) soundings (00 UTC, 12 UTC) for July 2016 are presented.

The deep layer vertical wind shear (e.g. 0 to 6 km) is also an important parameter by influencing both the type and movement of multicell DMC systems and their precipitation efficiency, which is the ratio of the accumulated precipitation at the surface and the flux of water vapour upward through the cloud base. This deep layer wind shear is not taken into account in the present report, but as a preparation for possible future inclusion of deep layer wind shear in I_{cb} an Appendix is added, giving a schematic overview of the impact of unidirectional and non-unidirectional vertical wind shear on development and movement of multicell Deep Moist Convection (DMC). The Appendix also contains a short summary of other factors (not a complete list) that may contribute to development of multicell DMC's with a cloud burst/flash-flood potential.

2 Method

In the present report a cloud burst/flash-flood index is defined as a combination of indicators, involving at most six out of the eight indicators, described in the list below:

- f_1: Vertically integrated water vapour divided by vertically integrated water vapour at saturation (potential vertically integrated water vapour)
- f_2: Vertically integrated water vapour
- f_3: Steering level wind (for example at 700 hPa)
- f_4: Convective INhibition (CIN)
- f_5: Convective Available Potential Energy (CAPE)
- f_6: Pressure difference between Level of Free Convection (LFC) and Equilibrium Level (EL)
- f_7: K-index (e.g. Bluestein, 1993)
- f_8: Thunder-storm index (Nielsen and Petersen, 2003)

Each indicator f_i depends on $\tanh(\eta_i)$, where $\eta_i = a_0 + c_i(p_i/pth_i - 1)$ and $c_i = a_0/(1 - p_{i*}/pth_i)$. With $a_0 = 0.5 \cdot \ln(3)$ the latter relations imply that $\tanh(\eta_i) = 0.5$ for the threshold $p_i = pth_i$ and equal zero for $p_i = p_{i*}$.

3 Indicators for severe DMC

The index I_{cb}, defined in Section 4, consists of indicators for dynamics, f_{dyn}, thermodynamics, f_{tdyn}, and for the moisture content of the troposphere, f_{moist}.

The indicator f_1 is defined as

$$f_1 = \max(0, \tanh(\eta_1)), \quad \eta_1 = a_0 + c_1 \left(\frac{p_1}{pth_1} - 1 \right), \tag{1}$$

where $p_1 = (q_{vint}/q_{svint})$ is the ratio of the vertically integrated water vapour to the value at saturation and $c_1 = a_0/(1 - p_{1*}/pth_1)$ with $p_{1*} = 0.2$ and $pth_1 = 0.4$, giving $c_1 = \ln(3)$.

The indicator f_2 is defined as

$$f_2 = \max(0, \tanh(\eta_2)), \quad \eta_2 = a_0 + c_2 \left(\frac{p_2}{pth_2} - 1 \right) \tag{2}$$

where p_2 is the vertically integrated water vapour in $\mathrm{kg\,m^{-2}}$ and $c_2 = a_0/(1 - p_{2*}/pth_2)$ with $p_{2*} = 14\,\mathrm{kg\,m^{-2}}$ and $pth_2 = 18\,\mathrm{kg\,m^{-2}}$, giving $c_2 = \frac{9}{4}\ln(3)$. The indicator for the moisture content in the troposphere is then defined as

$$f_{moist} = (f_1 \cdot f_2)^{1/2}. \tag{3}$$

This definition takes into account that the precipitation efficiency for a fixed value of vertically integrated water vapour in the troposphere tends to increase with increasing relative humidity (Markowski and Richardson, 2010).

The indicator f_3 is defined as

$$f_3 = \max(0, 1 - \tanh(\eta_3)), \quad \eta_3 = a_0 + c_3 \left(\frac{p_3}{pth_3} - 1 \right), \tag{4}$$

where p_3 is the wind speed in $\mathrm{m\,s^{-1}}$ at 700 hPa (assumed to be a typical steering level for DMC cells) and $c_3 = a_0/(1 - p_{3*}/pth_3)$ with $p_{3*} = 0\,\mathrm{m\,s^{-1}}$ and $pth_3 = 20\,\mathrm{m\,s^{-1}}$, giving $c_3 = \frac{1}{2}\ln(3)$. Note that $f_3 = 1$ if the steering level wind speed is zero and approaches zero asymptotically for large wind speeds. The effect of deep layer vertical wind shear on the movement of multicell DMC's, as described in the Appendix, is not taken into account at present. The motion vector of multicell DMC systems is assumed to be identical to the wind velocity at the steering level, which is the motivation for

$$f_{dyn} = f_3. \tag{5}$$

The indicator f_4 is defined as

$$f_4 = \max(0., 1 - \tanh(\eta_4)), \quad \eta_4 = a_0 + c_4 \left(\frac{p_4}{pth_4} - 1 \right), \tag{6}$$

where p_4 is the Convective INhibition (CIN) in $\mathrm{m^2 s^{-2}}$, $c_4 = a_0/(1 - p_{4*}/pth_4)$ with $p_{4*} = 0\,\mathrm{m^2 s^{-2}}$ and $pth_4 = -50\,\mathrm{m^2 s^{-2}}$, giving $c_4 = \frac{1}{2}\ln(3)$. Note that $f_4 = 1$ if $\mathrm{CIN} = 0$ and approaches zero asymptotically for large $-\mathrm{CIN}$.

The indicator f_5 is defined as

$$f_5 = \max(0, \tanh(\eta_5)), \quad \eta_5 = a_0 + c_5 \left(\frac{p_5}{pth_5} - 1 \right), \tag{7}$$

where p_5 is the Convective Available Potential Energy (CAPE) in $\mathrm{m^2 s^{-2}}$ and $c_5 = a_0/(1 - p_{5*}/pth_5)$ with $p_{5*} = 0\,\mathrm{m^2 s^{-2}}$ and $pth_5 = 100\,\mathrm{m^2 s^{-2}}$, giving $c_5 = \frac{1}{2}\ln(3)$. A variable value of $pth_5 = 10 \cdot (19 - 18 \cdot f_2)$, depending on how close to saturation the troposphere is, has been proposed as an alternative choice. Note that $f_5 = 0$ if $\mathrm{CAPE} = 0$ and approaches 1 asymptotically for large values of CAPE.

The indicator f_6 is defined as

$$f_6 = \max(0, \tanh(\eta_6)), \quad \eta_6 = a_0 + c_6 \left(\frac{p_6}{pth_6} - 1 \right), \tag{8}$$

where p_6 is the pressure difference in hPa from the Level of Free Convection (LFC) to the Equilibrium Level (EL), which is equivalent to the vertical Acceleration Path (AP) in hPa for DMC cells, and $c_6 = a_0/(1 - p_{6*}/pth_6)$ with $p_{6*} = 0\,\mathrm{hPa}$ and $pth_6 = -50\,\mathrm{hPa}$, giving $c_6 = \frac{1}{2}\ln(3)$. The index f_6 approaches 1 asymptotically for large AP's and is zero if AP is zero. Note that if $\mathrm{CAPE} = 0$, also CIN and AP are zero, which means that a "stable" sounding has $f_4 = 1$ and $f_5 = f_6 = 0$.

The indicator f_7 is defined as

$$f_7 = \max(0, \tanh(\eta_7)), \quad \eta_7 = a_0 + c_7 \left(\frac{p_7}{pth_7} - 1 \right), \tag{9}$$

where p_7 is the K-index (e.g. Bluestein, 1993), and $c_7 = a_0/(1 - p_{7*}/pth_7)$ with $p_{7*} = 26$ and $pth_7 = 28$, giving $c_7 = 7 \cdot \ln(3)$. The index f_7 approaches 1 asymptotically for large values of the K-index and is zero for $p_7 = p_{7*}$.

The last indicator, f_8, is actually an index for thunder storms, based on maximum CAPE obtained by calculating CAPE as function of lifting level below 500 hPa (for details: see Nielsen and Petersen, 2003).

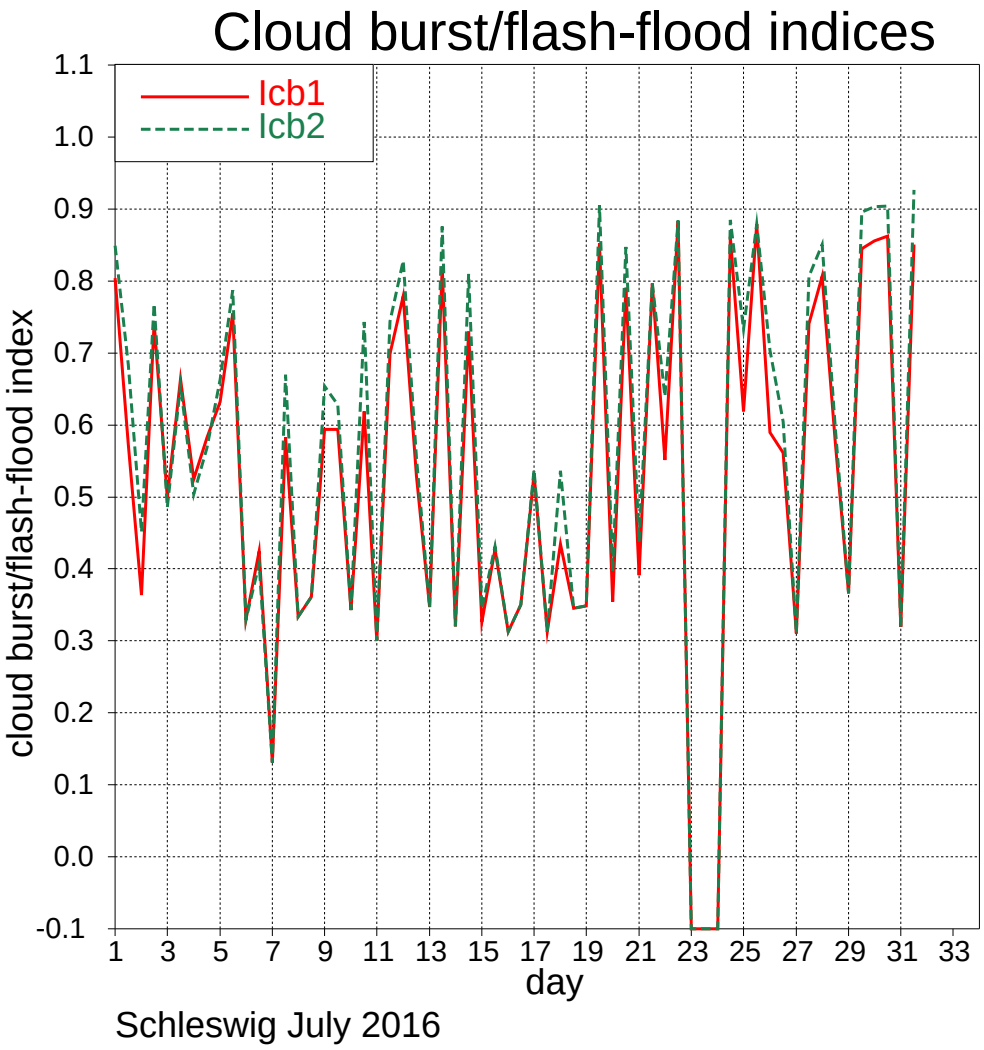

Figure 1: Intra-monthly 12-hourly variation in cloud burst/flash-flood indices I_{cb1} and I_{cb2}. In I_{cb1} the threshold for CAPE is constant, while it is a function of f_2, the indicator for vertically integrated water vapour, in I_{cb2} (see text for details). A negative value (-0.1) of I_{cb} means that sounding data is missing. Soundings are available 00 and 12 UTC from University of Wyoming (Weather.uwyo.edu/upperair).

4 The cloud burst/flash-flood index

The cloud burst/flash-flood index is calculated as

$$I_{cb} = {f_{moist}}^{\delta_1} \cdot {f_{dyn}}^{\delta_2} \cdot {f_{tdyn}}^{\delta_3}, \tag{10}$$

where $\delta_i (i = 1, 2, 3)$ are weights with the constraint $\delta_1 + \delta_2 + \delta_3 = 1$. f_{moist} and f_{dyn} are given by (3) and (5), respectively, and f_{tdyn} is an indicator for thermodynamics. Among the indicators f_{tdyn} is likely to be the most uncertain, since it depends on details in the vertical profiles of temperature and specific humidity, including the surface values. For this reason different versions of f_{tdyn} have been tested in the present report. The versions are

$$f_{tdyna} = \max((f_4 \cdot f_5 \cdot f_6)^{1/3}, 0.05) \quad (11)$$
$$f_{tdynb} = \max((f_4 \cdot f_{5*} \cdot f_6)^{1/3}, 0.05) \quad (12)$$
$$f_{tdync} = \max((f_{4*} \cdot f_{5*})^{1/2}, 0.05) \quad (13)$$
$$f_{tdynd} = \max((f_4 \cdot f_5)^{1/2}, 0.05) \quad (14)$$
$$f_{tdynt} = f_8 \quad (15)$$

The threshold values in f_{4*} and f_{5*} are not constants as in f_4 and f_5, but functions of the indicator for vertically integrated water vapour, f_2, as specified in subsection 5.1. The indicators f_{tdyna}, f_{tdynb} and f_{tdync} have a positive lower limit, presently set to 0.05. Without the latter constraint $\mathrm{I_{cb}}$ based on these indicators would be zero even if both f_{moist} and f_{dyn} were close to 1. With the constraint above such a situation gives $I_{cb} \approx 0.05^{\delta_3}$.

It is important to note that I_{cb} generally does not account for cloud bursts/flash-floods generated along near-surface convergence lines or by DMC originating from a level above the PBL, the latter except in the case with $f_{tdyn} = f_{tdynt}$.

5 Preliminary results

5.1 Intra-monthly variation in I_{cb} for Schleswig in July 2016

Figure 1 shows the day to day variation of I_{cb} in steps of 12 hours for Schleswig in July 2016. The figure shows two variants of I_{cb}. Both variants use equation (10) with $f_{tdyn} = f_{tdyna}$, variant I_{cb1} uses f_5 with the constant threshold value $pth_5 = 100\,\mathrm{m^2 s^{-2}}$ and I_{cb2} uses f_{5*} withs $pth_5 = 10 \cdot (19 - 18 \cdot f_2)\,\mathrm{m^2 s^{-2}}$, which means that in variant I_{cb2} the threshold for CAPE varies with the vertically integrated water vapour in the troposphere in such a way that increasing moisture implies a decreasing threshold for CAPE. Both I_{cb1} and I_{cb2} use $\delta_1 = \delta_2 = \delta_3 = 1/3$. It can be seen from Figure 1 that I_{cb2} most of the time is a bit larger than I_{cb1}. The number of soundings with $I_{cb2} \geq 0.8$ is 15 (11 for the mid-day soundings and 4 for the midnight soundings), while the corresponding number for I_{cb1} is 11 (8 for the mid-day soundings and 3 for the midnight soundings). The larger numbers for the mid-day soundings are undoubtly due to normally increasing CAPE during day. I_{cb} values equal -0.1 mean that sounding data is missing.

All the cases presented in subsections 5.2, 5.3 and 5.4 show a cloud burst index, I_{cb3}, defined by (10) with $f_{tdyn} = f_{tdync}$, i.e. based on f_{4*} and f_{5*} with threshold values for CIN and CAPE that are functions of the indicator, f_2, for vertically integrated water vapour, and given by $pth_4 = -50(1 + 2{f_2}^2)$ and $pth_5 = \max(1, 190 - 180 f_2)$, respectively. Further subsections 5.2 and 5.3 show a bit simpler cloud burst index, I_{cb4}, calculated in the same way as I_{cb3}, except that the threshold values for CIN and CAPE are constants with values $\mathrm{pth_4} = -50\,\mathrm{m^2 s^{-2}}$ and $\mathrm{pth_5} = 100\,\mathrm{m^2 s^{-2}}$, respectively.

Section 7.5 contains an intercomparison of I_{cb3} and I_{cb5}. The latter is identical with I_{cb3}, except that $f_{tdyn} = f_{tdync}$ has been replaced by $f_{tdyn} = f_{tdynt}$. The section also contains an intercomparison of

the cloud burst indices I_{cb5}, I_{cb6}, I_{cb7} and I_{cb8}. The definitions of the indices are listed below.

$$I_{cb1} = (f_{moist} \cdot f_{dyn} \cdot f_{tdyna})^{1/3} \quad (16)$$
$$I_{cb2} = (f_{moist} \cdot f_{dyn} \cdot f_{tdynb})^{1/3} \quad (17)$$
$$I_{cb3} = {f_{moist}}^{0.4} \cdot (f_{dyn} \cdot f_{tdync})^{0.3} \quad (18)$$
$$I_{cb4} = {f_{moist}}^{0.4} \cdot (f_{dyn} \cdot f_{tdynd})^{0.3} \quad (19)$$
$$I_{cb5} = {f_{moist}}^{0.4} \cdot (f_{dyn} \cdot \max(f_{tdynt}, 0.05))^{0.3} \quad (20)$$
$$I_{cb6} = 0.5 \cdot (I_{cb3} + f_{tdynt}) \quad (21)$$
$$I_{cb7} = {f_{moist}}^{0.4} \cdot (f_{tdync} \cdot f_{tdynt})^{0.3} \quad (22)$$
$$I_{cb8} = {f_{moist}}^{0.4} \cdot (f_{dyn} \cdot f_{tdynt})^{0.3} \quad (23)$$

5.2 The severe cloud burst event in Copenhagen on 2nd July 2011

In the early evening on 2nd July 2011 a severe cloud burst occurred in the Copenhagen area. Between 90 and 135 mm of precipitation in less than 2 hours was recorded in the central part of the city. During the late afternoon deep moist convection (DMC) developed over Skåne (the southernmost part of Sweden) in an air stream from east-northeast. In the early evening the DMC passed over Øresund to Copenhagen, where it created a severe flash flood.

The cloud burst index, I_{cb3}, for this case is shown in Figure 2. According to the latter figure the index is rather consistent for all the four forecasts valid at 18 UTC on 2nd July, but run from four different initial times, separated by 6-hourly steps, beginning 1 July 18 UTC. In I_{cb3} the threshold values for CIN and CAPE decrease numerically with increasing vertical integrated water vapour, giving larger cloud burst indices than with the constant threshold values in I_{cb4}. This is clearly seen by intercomparison of Figure 2 and Figure 3 that shows equivalent figures for I_{cb1}.

The index must be regarded as a property of the combined air mass and underlying surface characteristics, showing its potential for generating cloud bursts, but the index is unable to give accurate locations for cloud burst generations. This is illustrated in Figure 2, where 'spots' with $I_{cb3} > 0.9$ are seen over southern Sweden. Their locations vary with forecast lead time, and no cloud bursts were reported at these locations. The index seems to give a necessary, but insufficient condition for development of organised DMC's leading to cloud burst/flash flood. In some cases this organisation may be controlled by stationary forcing that creates surface convergence lines on meso- to sub-meso scale. Horizontal and vertical shear of the environmental wind can also lead to development of deep moist convective systems, as discussed in the Appendix.

The index shows the focus areas with potential for cloud burst/flash flood generation, but is unable to point precisely to where cloud burst development will occur. This is related to the low predictability og cloud burst generating DMC's. Other kinds of information, not least from radars and satellites, may help to localise cloud burst initiation, but usually only a short time (up to a few hours) in advance.

The focus areas are considered to be where I_{cb3} has values above 0.75. Below this value the potential for generation of cloud bursts is considered to be small. Forecasters may use such knowledge to concentrate their main attention on the focus areas. Figure 2 shows that I_{cb3} over Copenhagen and upstream over southern Sweden has mostly values between 0.8 and 1, indicating a moderate to high potential/risk for development of cloud bursts within these regions. In the Copenhagen area I_{cb3} is somewhat lower in the 24 h forecast than in the 18, 12 and 6 h forecasts. The last sub-figure (bottom right) in Figure 2 shows an overall significant decrease in I_{cb3} in the high-index areas from the

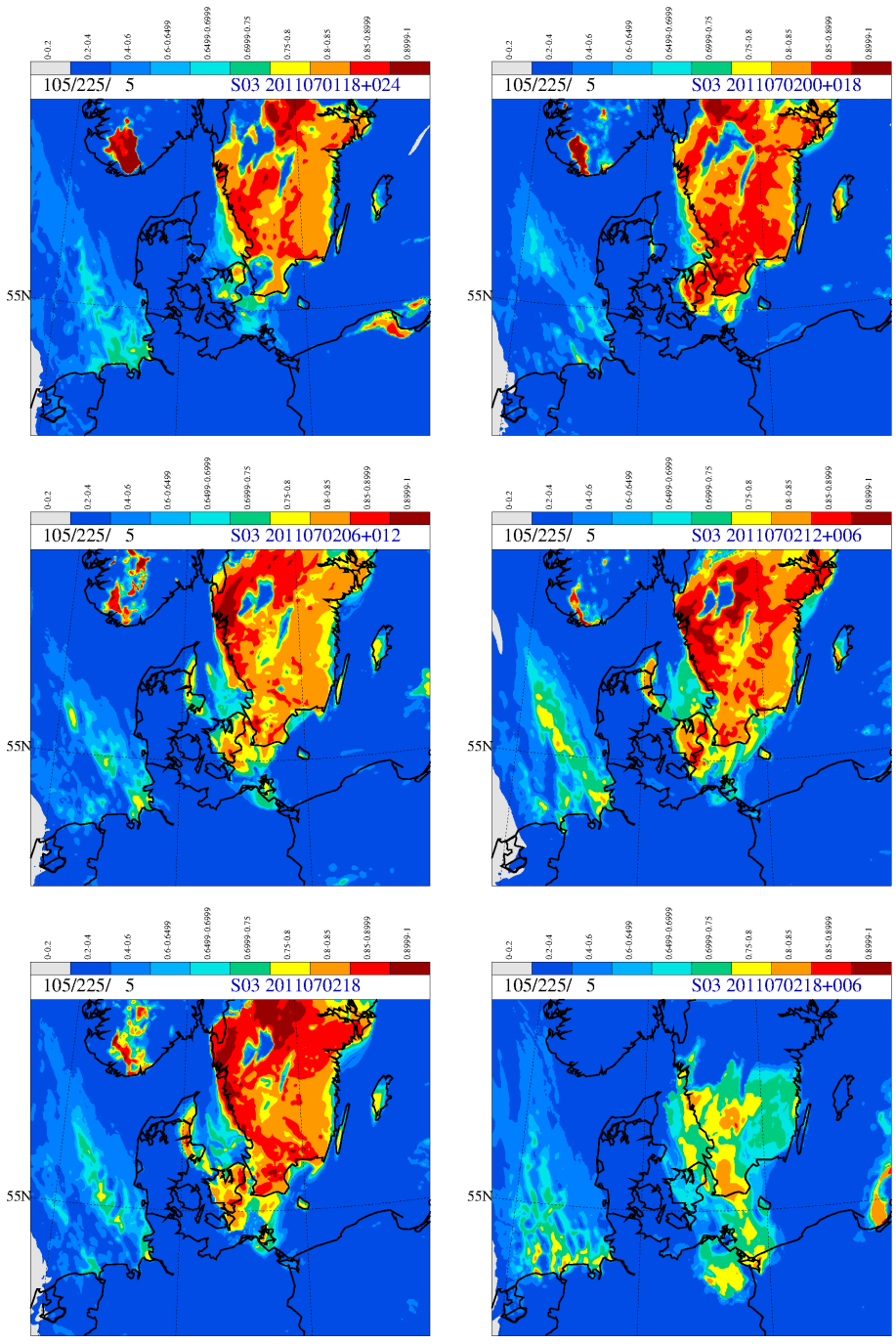

Figure 2: Cloud burst index $f_{cbi} = I_{cb3}$ valid 18 UTC on 2 July 2011. Top: 18 h forecast, bottom: verifying analysis. Colour intervals in steps of 0.2 until 0.6, thereafter in steps of 0.05 until 0.9. The last (dark red) interval is from 0.9 to 1 (the maximum index value). In the early evening on 2 July a severe cloud burst occurred in central Copenhagen.

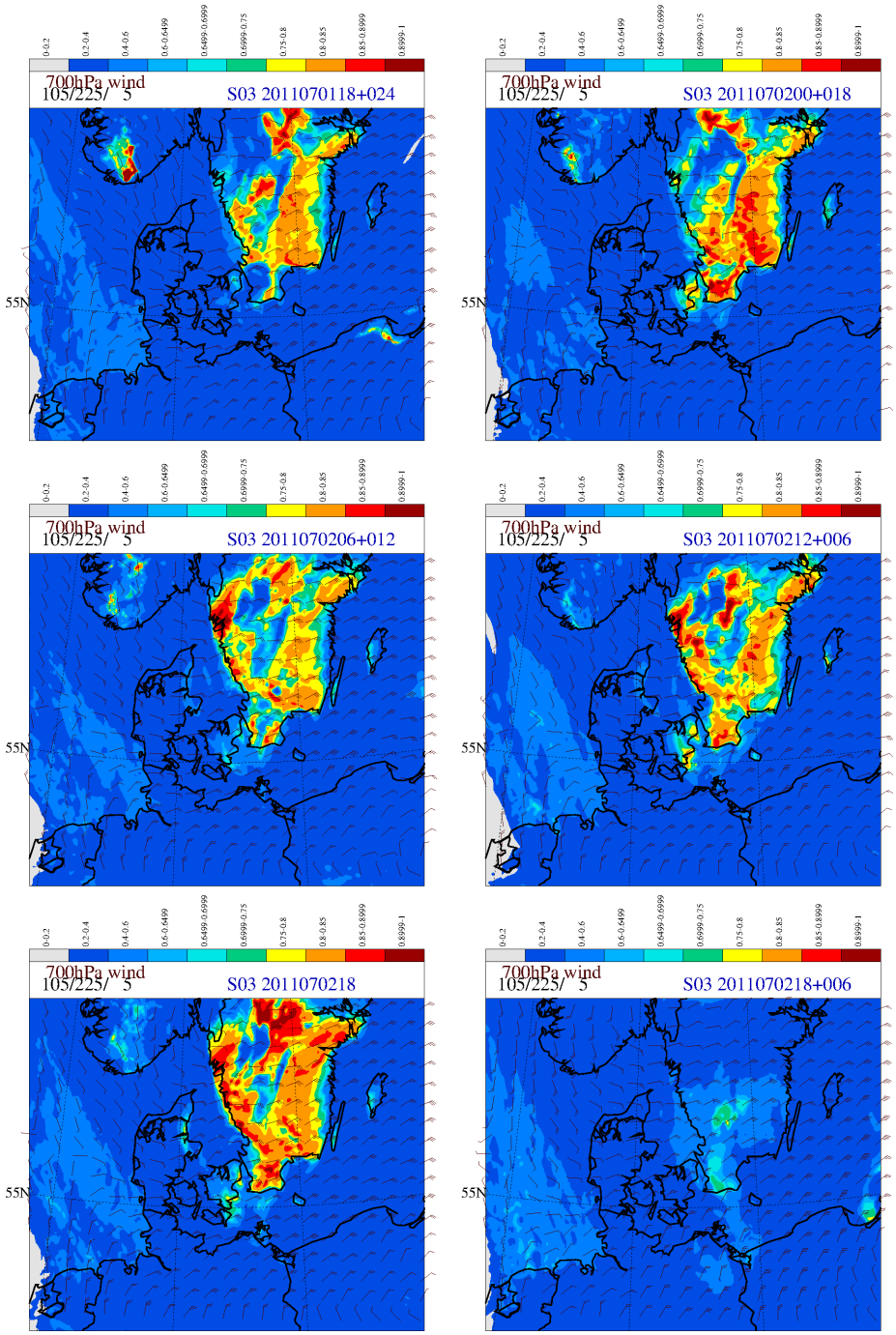

Figure 3: As Figure 2, but for cloud burst index $f_{cbi} = I_{cb1}$, and with wind velocity (WMO standard) at 700 hPa.

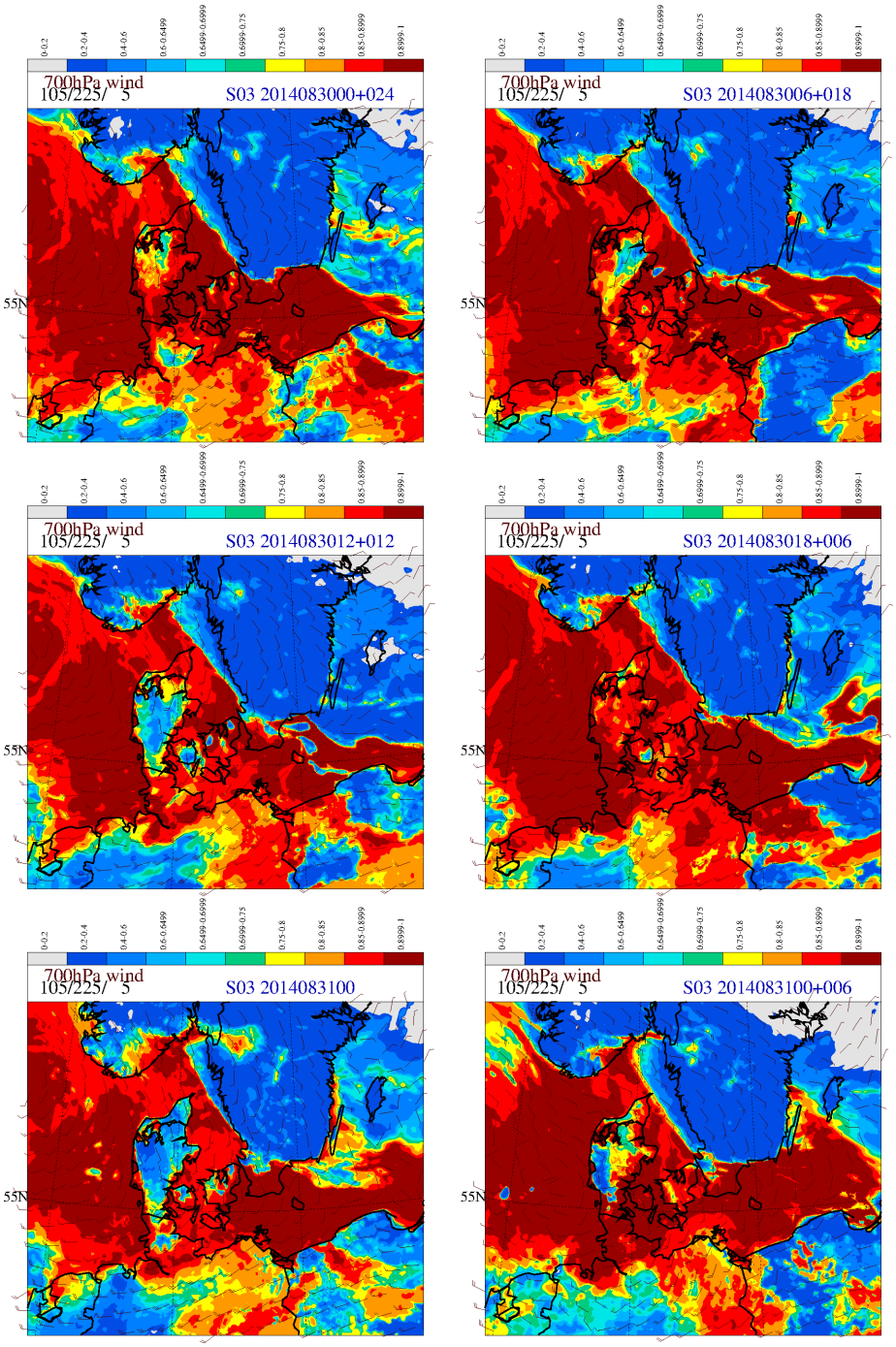

Figure 4: Cloud burst index $f_{cbi} = I_{cb3}$ valid 00 UTC on 31 August 2014. Top: 18 h forecast, bottom: verifying analysis. Colour intervals in steps of 0.2 until 0.6, thereafter in steps of 0.05 until 0.9. The last (dark red) interval is from 0.9 to 1 (the maximum index value). The arrows show wind velocity (WMO standard) at 700 hPa. Between 00 and 03 UTC on 31 August a severe cloud burst occurred in Copenhagen and 1 to 2 hours later in the Malmø region.

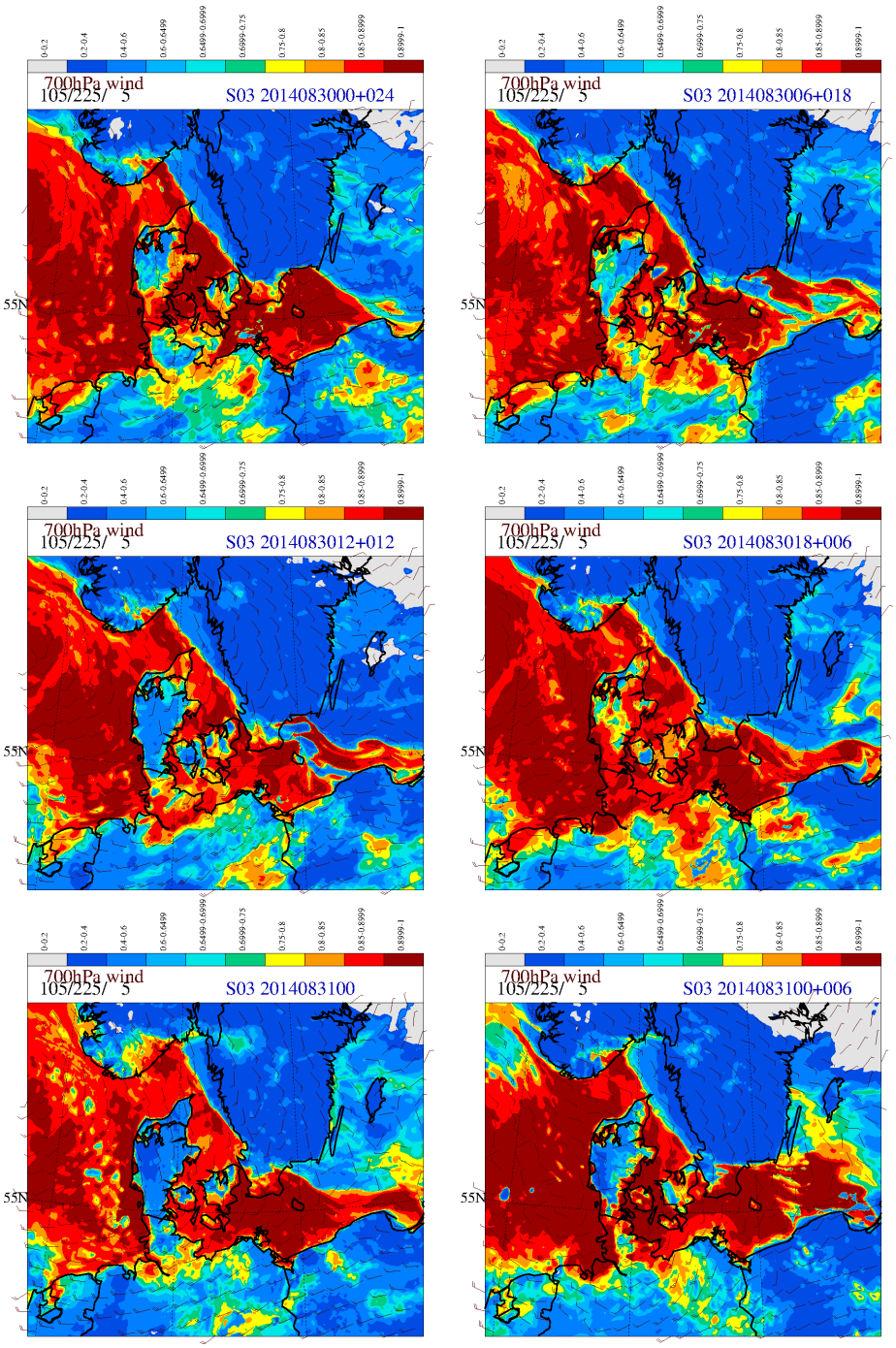

Figure 5: As Figure 4, but for cloud burst index $f_{cbi} = I_{cb1}$.

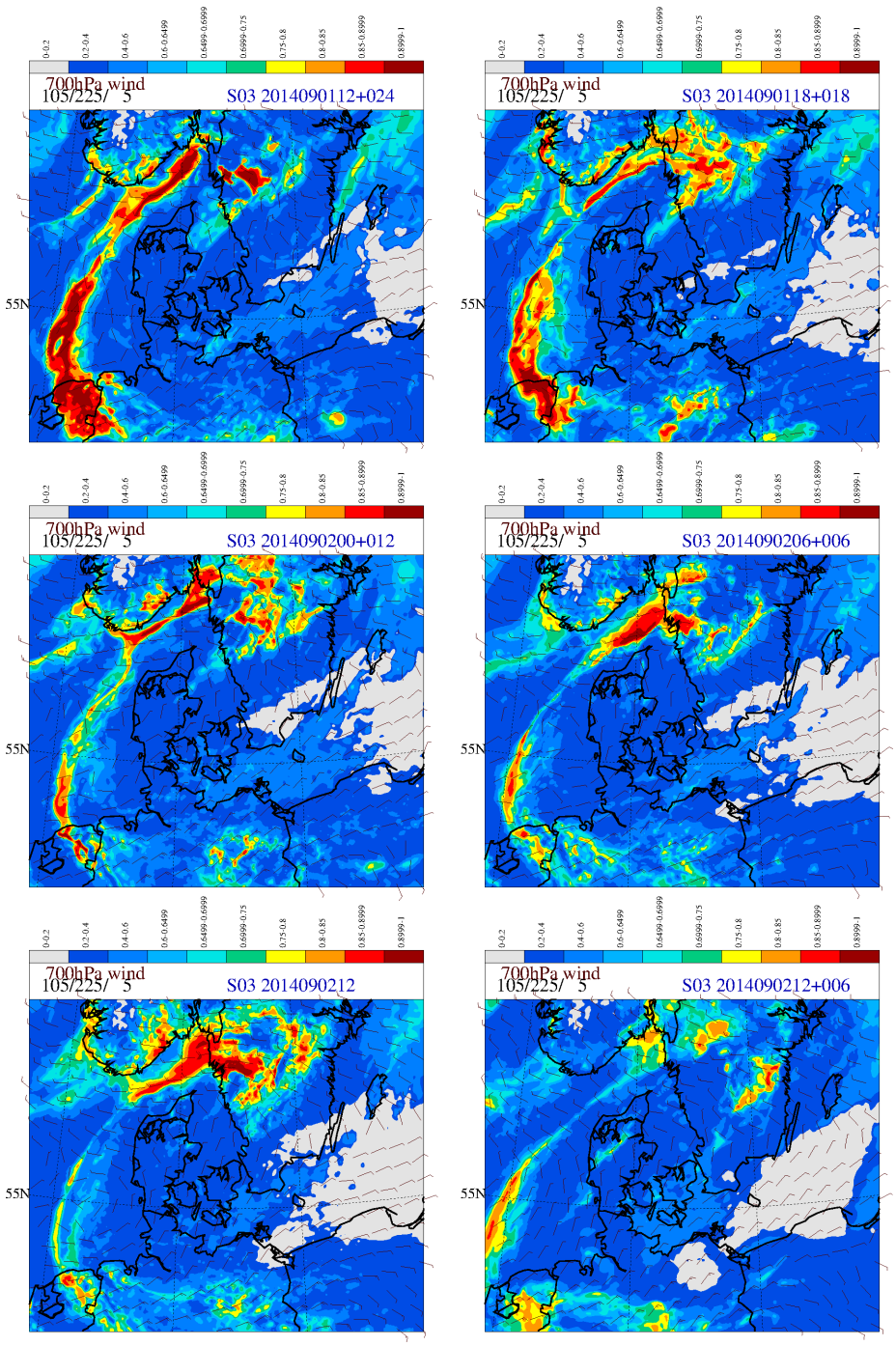

Figure 6: Cloud burst index $f_{cbi} = I_{cb3}$ valid 12 UTC on 2nd September 2014. Top: 18 h forecast, bottom: verifying analysis. Colour intervals in steps of 0.2 until 0.6, thereafter in steps of 0.05 until 0.9. The last (dark red) interval is from 0.9 to 1 (the maximum index value). The arrows show wind velocity (WMO standard) at 700 hPa. No cloud burst occurred over Denmark on this day. Radar reflectivity images indicate precipitation at 12 UTC in the "red spot" area north of Jutland.

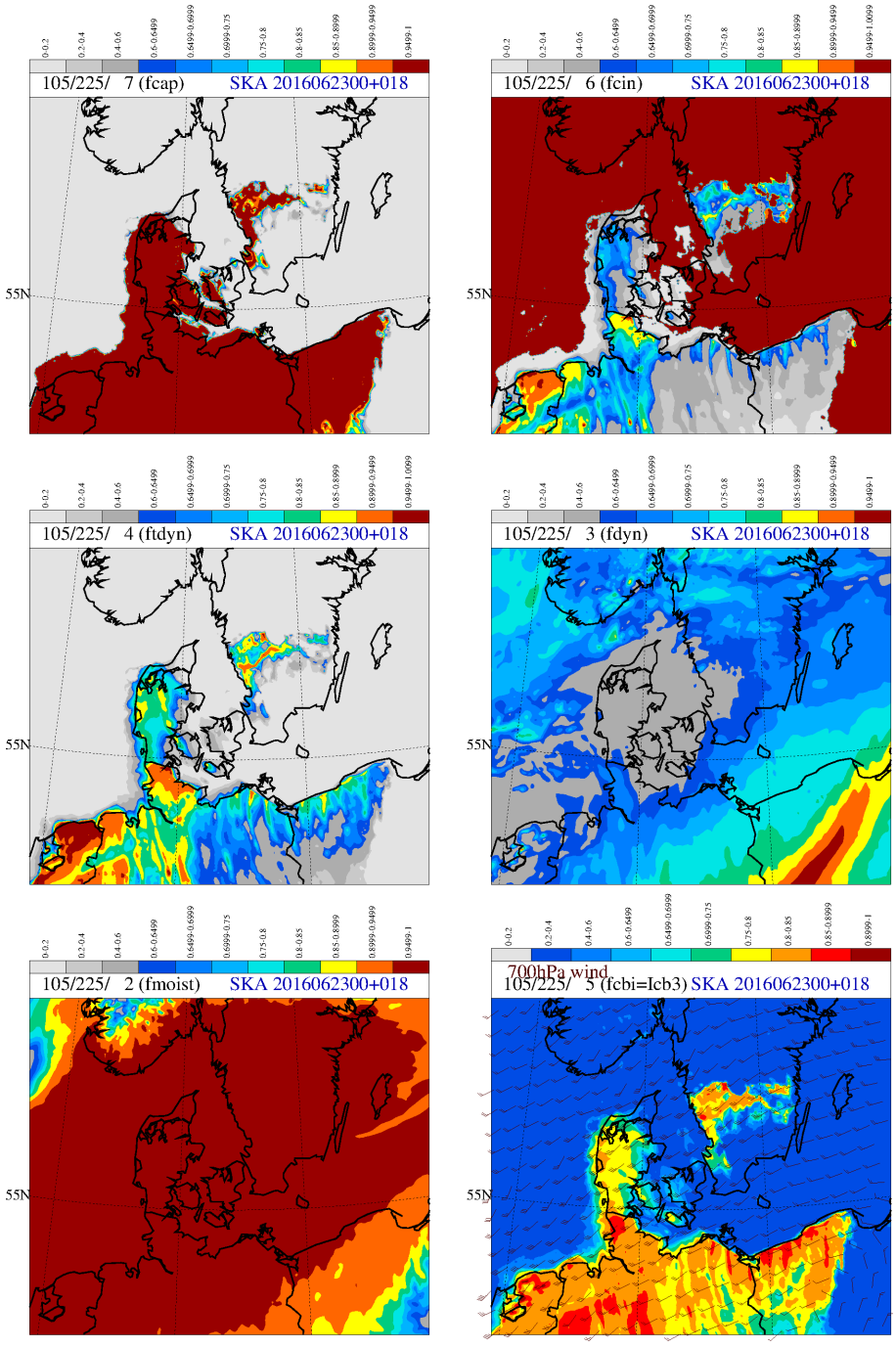

Figure 7: 18 h forecasts, valid 18 UTC 23 June 2016, of five cloud burst indicators and the cloud burst index, all with values between 0 and 1. From top left f_{cap}, f_{cin}, f_{tdyn}, f_{dyn}, f_{moist} and bottom right $f_{cbi} = I_{cb3}$

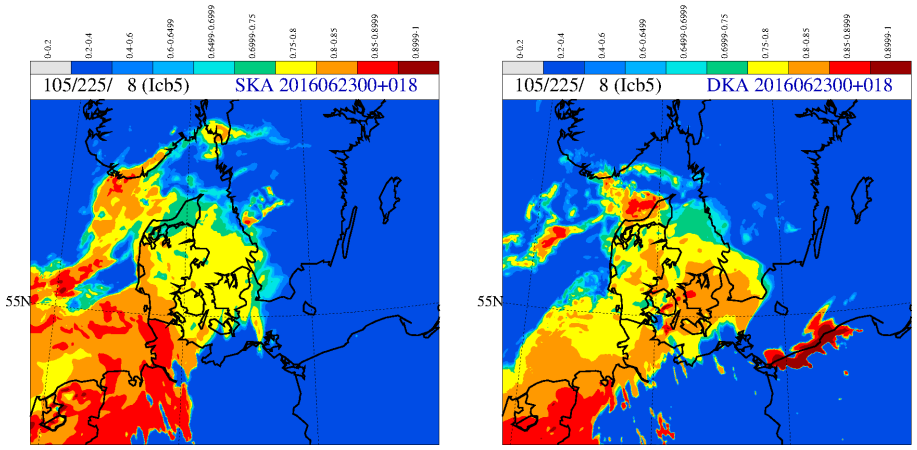

Figure 8: 18 h forecasts of cloud burst index I_{cb5}, valid 18 UTC 23 June 2016. Left: DMI-HIRLAM-SKA, right: DMI-HARMONIE-DKA.

analysis at 18 UTC to the 6 h forecast valid at midnight 3 July. Radiative cooling of the land surface and dry air advection from central Scandinavia contributes to the decrease of the index. For intercomparison a bit simpler cloud burst index, I_{cb1}, is shown in Figure 3. The latter index has - contrary to I_{cb3} - constant threshold values for CIN and CAPE. Since these threshold values in I_{cb3} become smaller with increasing vertically integrated water vapour it is expected that the index I_{cb3} is higher than I_{cb1} if the troposphere has a sufficiently high moisture content. This is confirmed by intercomparison of Figure 2 and Figure 3.

5.3 The strong cloud burst event in Copenhagen 31 August 2014

This event tells much the same story as Figure 2. The I_{cb3} in Figure 4 is fairly consistent for all the four forecasts valid at 00 UTC on 31 August. $I_{cb3} > 0.9$ occurs consistently in large regions over the North Sea and the eastern Baltic, including Øresund and the southern part of Skåne. Smaller and less consistent spots are present elsewhere in the Danish Waters. Within a few hour period from around midnight several DMC cells developed mainly over the sea south of Copenhagen and moved with a steering wind from south across the central city. In less than two hours more than 100 mm of rain was measured at some locations in the city. Later in the night the heavy precipitation cells drifted eastward to the Malmø area in Skåne. According to Figure 4 a clear potential for cloud bursts were present in the area hit by cloud bursts both in the 24, 18, 12 and 6 h forecasts. Also other regions had a potential for cloud burst development, but no cloud bursts were recorded in those regions. Figure 5 shows the cloud burst index I_{cb4}. As in the previously shown July case the I_{cb4} index has generally lower values than I_{cb3}.

5.4 A case without cloud bursts 2 September 2014

Figure 6 shows the cloud burst index I_{cb3} on a day without any cloud burst reports in Denmark. The figure shows low values, except in a narrow band from the Netherlands over the eastern North Sea and Scagerac to Götaland in Sweden. According to radar reflectivity images there were scattered DMC's, but no sign of cloud burst development in this band. Like in the two previous shown cases there is a high degree of consistency from forecast to forecast.

5.5 A weak cloud burst case 23 June 2016

During the afternoon and evening on 23 June 2016 several DMC's developed in a humid southwesterly air stream over Denmark (Figure 7, bottom left). The cloud burst index I_{cb3} (Figure 7, bottom-

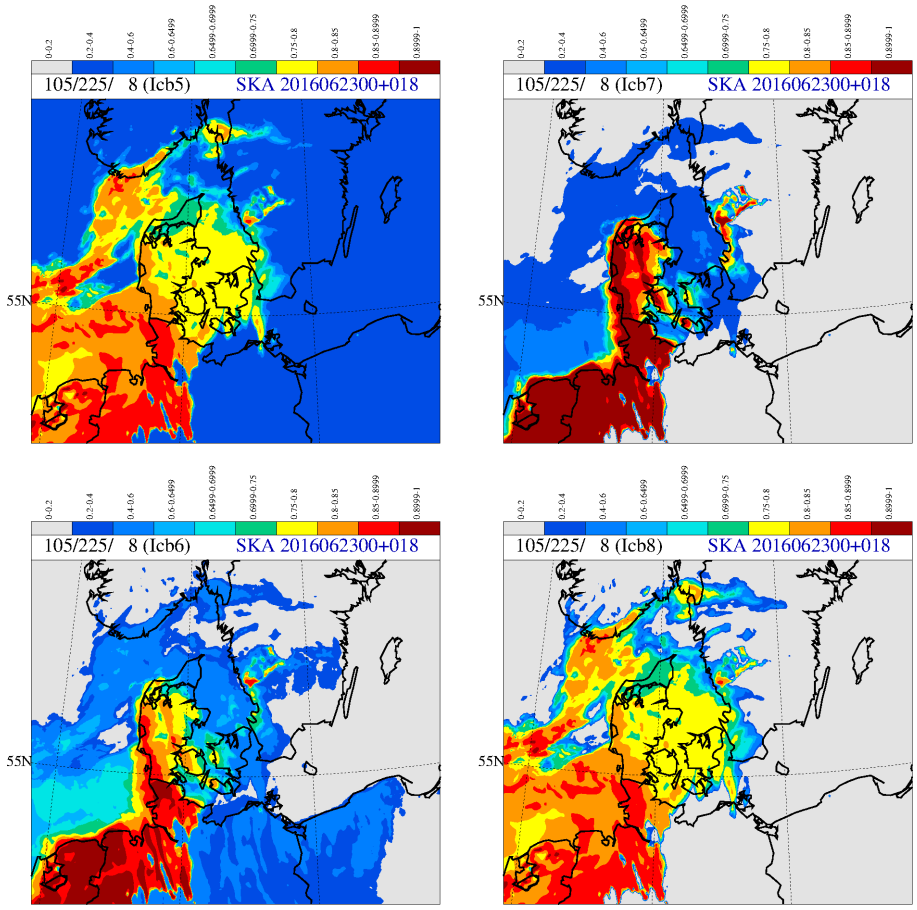

Figure 9: 18 h DMI-HIRLAM-SKA forecasts of four different cloud burst indices, valid 18 UTC 23 June 2016. Top-left: I_{cb5}, top-right: I_{cb7}, bottom-left: I_{cb6} and bottom-right: I_{cb8}

right) indicates that the conditions were only moderately favourable for cloud burst development (Figure 7, bottom-right), mainly due to relatively high steering level winds (Figure 7, middle-right) and relatively large CIN (Figure 7, top-right). Measurements of accumulated precipitation showed that the cloud burst limit (defined as at least 15 mm of precipitation in 30 minutes) between 17 and 19 UTC was exceeded locally in the Great Belt area (Tåsinge, Langeland, southwest Zealand and the western part of Lolland). The limit was only exceeded marginally, and after 19 UTC there were no more reports of cloud bursts in Denmark.

Presently, on-duty forecasters at DMI have access to two operational DMI-NWP models (DMI-HARMONIE and DMI-HIRLAM), having I_{cb} as an output parameter. Figure 8 shows 18 h I_{cb5} cloud burst forecasts valid 18 UTC 23 June 2016 produced by DMI-HIRLAM-SKA (left) and by DMI-HARMONIE-DKA (right). The forecasts are not identical, but have a large overlap of regions with an index larger than 0.75. One exception is a narrow region at the Baltic Sea coast of Poland. Here SKA has low and DKA high values of the index. For the same forecast lead time and the same valid time as in Figure 8 cloud burst indices based on I_{cb5}, I_{cb6}, I_{cb7} and I_{cb8} are intercompared in Figure 9. The top-left and bottom-right sub-figures show the effect of imposing a lower limit on the indicator for thermodynamics (here f_{tdynt}). The effect is primarily to increase small index values (shown by a

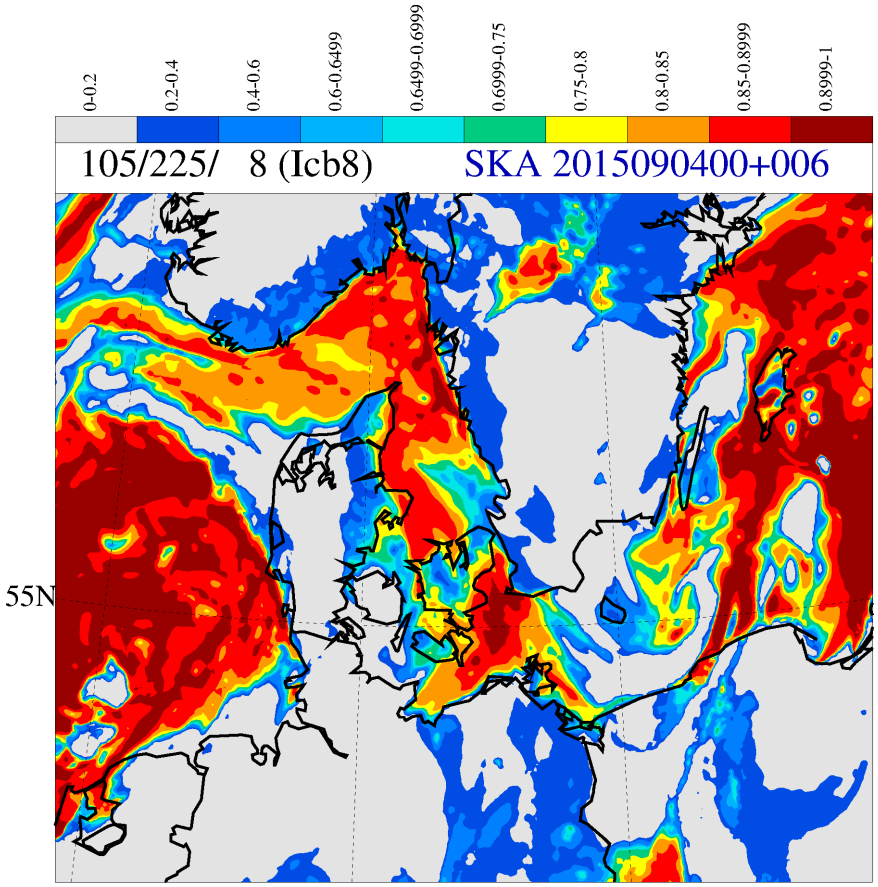

Figure 10: 6 h forecast, valid 6 UTC 4 September 2015

colour shift from grey in the bottom-right sub-figure to blue in the top-left sub-figure), and leave the high values nearly unaffected.

Intercomparison of the top-left and bottom-left sub-figure shows mainly the effect of including in the cloud burst index both the thermodynamic indicator f_{tdync} and f_{tdynt} (the thunder-storm index). This is done in I_{cb6}. With inclusion of f_{tdynt} in I_{cb6} the area with high index values (> 0.75) is reduced, but within the region with $I_{cb6} > 0.75$ the index is mostly higher than the I_{cb5} index.

A similar effect is obtained in I_{cb7} (Figure 9, top-right), where f_{dyn} has been replaced by f_{tdync}. This can be seen by intercomparing sub-figures top-right and bottom-left in Figure 9. Inside the regions in sub-figure top-right with an index larger than 0.75, sub-figure bottom-left has mostly lower index values and sub-figure top-left mostly the lowest index values.

5.6 A rain/hail cloud burst in Copenhagen 4 September 2015

In this case DMC's developed rapidly, first over land west of Copenhagen and shortly after over the sea south of Copenhagen. The first cells were detected by radar only about 1 hour prior to to the cloud burst in Copenhagen. It was therefore considered as a case with very low predictability.

A 6 h forecast of the cloud burst index, I_{cb8}, valid 6 UTC 4 September, is shown in Figure 10. It has high values over the sea south of Copenhagen, showing a potential for cloud burst development in this region. Between 30 and 60 mm of rain was recorded from 6 to 18 UTC in the southwestern part of Jutland, but the rain intensity was well below the cloud burst limit. During the latter period I_{cb8} was

below 0.6 over most of Jutland, and only with local spots with values up to 0.85 (Figures not shown). It is likely that availability of the I_{cb8} parameter on the day would have been beneficial for the on-duty forecasters, by focusing their attention more to the high cloud burst risk areas, not least the area south of Copenhagen, than to the precipitation area in the southwestern part of Jutland.

6 Conclusion

The present report presents a number of cloud burst indices that depend on moisture distribution and dynamic and thermodynamic properties of the troposphere and its underlying surface. Eight variants have been defined. Two of them, containing an indicator for the length of the acceleration path (from level of free convection to the equilibrium level) by lifting of air from the surface, have been tested for July 2016 soundings from Schleswig in northern Germany.

DMI-HIRLAM forecasts of the six other indices are shown for one or more cases. In all cases, except one, at least one cloud burst was recorded in Denmark. In all the cases with observed cloud bursts the indices showed a potential for cloud burst generation at the locations where it occurred, but there were also some regions with predicted cloud burst potential, where no burst were observed.

In the single case without cloud burst observations the forecasted indices showed no potential for cloud burst generation. It is also promising that no cloud bursts were observed outside the high-risk zones forecasted by the cloud burst indices in any of the presented case studies.

The presented results showed significant differences between the various indices. More experimentation is therefore needed to find 'the best' index. The presented case studies are too few to allow an estimate about false alarm rates. It is expected that such an estimate can be obtained from semi-operational forecasts of one or more cloud burst indices for the cloud burst season 2017 (in Denmark lasting from April to November).

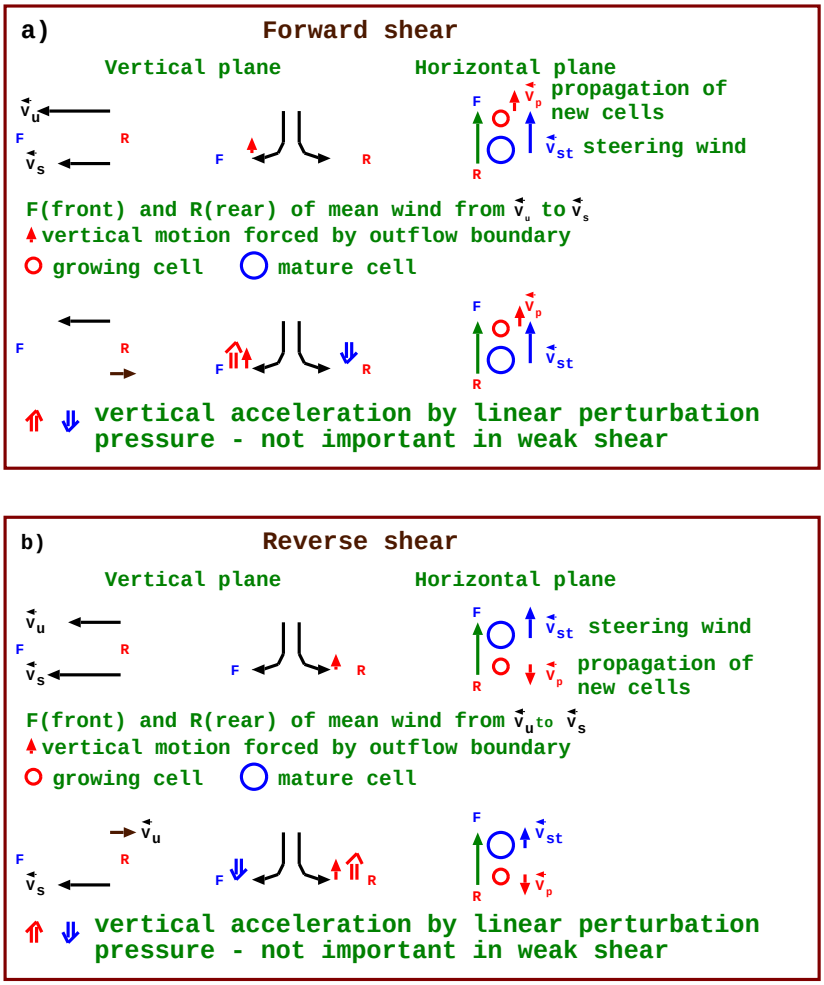

Figure 11: Schematics of induced vertical motion and resulting new convective cell formation due to interaction of the ambient flow with convective cells in unidirectional vertical wind shear a) in forward shear and b) in reverse shear. Diverging black arrows symbolise outflow from a mature cell. F and R are defined relative to the steering level wind, $\vec{V}_{st}$, supposed to be the level of mean wind velocity in the layer from level s to level u. Other symbols are explained in the figure.

7 Appendix

7.1 The influence of unidirectional vertical wind shear on development of multicell deep moist convection

Let $\vec{V}_s$ be a wind velocity in the Planetary Boundary Layer (PBL), $\vec{V}_u$ an upper-level wind velocity and $\vec{V}_{st}$ the steering level wind velocity, roughly representing the mean wind in the layer from level $'s'$ to level $'u'$. Next, consider for simplicity a uniform horizontal flow with unidirectional shear. Then the shear vector $\Delta\vec{V} = \vec{V}_u - \vec{V}_s$ with magnitude $S = |\Delta\vec{V}|$ is parallel to both $\vec{V}_s$,$\vec{V}_{st}$ and $\vec{V}_u$. The shear is defined to be **forward** if the mean wind ($\vec{V}_{st}$) is parallel to and in the direction of $\Delta\vec{V}$ and to be **reverse** if the mean wind is in the opposite direction of $\Delta\vec{V}$ (Duncan, 1978). Levels $'s'$, $'st'$ and $'u'$ could typically be 925, 700 and 500 hPa, respectively. Interaction between the ambient flow and the flow induced by Deep Moist Convection (DMC) generates both Linear Perturbation Pressure (LPP) and Non-Linear Perturbation Pressure (NLPP) that play significant roles in how DMC develops and behaves after initiation. NLLP only becomes important in strong shear with $S \geq 20, \mathrm{m\,s^{-1}}$, while LPP also has an impact in moderate shear with $S \geq 10\,\mathrm{m\,s^{-1}}$ (Markowski and Richardson, 2010). In cases with weak or no shear and sufficiently unstable air new convective cells can form randomly

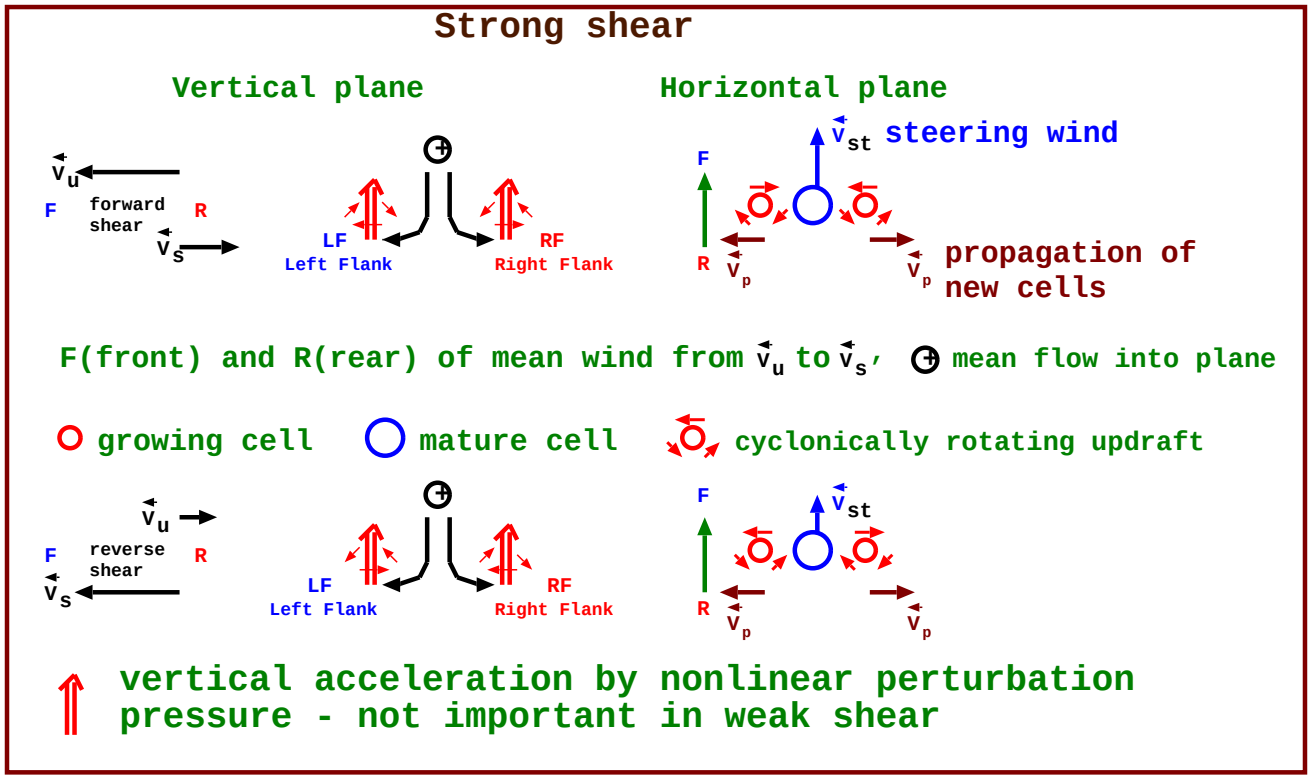

Figure 12: Schematics of induced vertical motion and resulting new convective cell formation due to interaction of the ambient flow with convective cells in unidirectional vertical strong wind shear. Top and bottom schematics show a case with forward and reverse shear, respectively. Diverging black arrows symbolise outflow from a mature cell. Other symbols are explained in the figure. Both cases show storm splitting. In reverse shear the left and right moving updrafts rotate in opposite directions of the rotating updrafts in forward shear. Symbols not explained have the same meaning as in Figure 11

by dynamical lifting of air along outflow boundaries from mature cells. This type of DMC shows little or no organisation and generation of cloud bursts are not so likely. A night picture of a DMC cell with an overshooting top is shown in Figure 14.

As **forward** shear increases, the dynamical lifting of air along an outflow boundary becomes largest downshear of a mature cell. Consequently, the outflow boundary in front of the mature cell becomes the preferred region of new cell formation and adds a propagation velocity $\vec{V}_p$ to and in the direction of $\vec{V}_{st}$ (Figure 11a, top). As the **forward** shear further increases to moderate values, LPP becomes significant. It generates upward acceleration of air on the downshear side of the mature cell (Klemp,1987; Nielsen, 2006) and therefore favours growth of new cells in the region which also has the largest lifting along the outflow boundary of the mature cell (Figure 11a, bottom). The **forward** shear forms a forward building multicell system that moves faster than the individual cells. In **reverse** shear the favoured region of largest outflow boundary forcing and upward acceleration by LPP is on the upwind (downshear) side of the mature cell (Figure 11b). The added $\vec{V}_p$ is in the opposite direction of $\vec{V}_{st}$. Consequently, **reverse** shear forms a backward building multicell system that moves slower than the individual cells. These results indicate that at a given $\vec{V}_{st}$ and for cells with identical precipitation intensities a cloud burst/flash-flood is more likely in **reverse** than **forward** shear, simply due to the slower motion of the reverse shear system.

In cases with strong shear (Figure 12) non-linear pressure perturbations become the strongest forcing terms. They create supercell storm splitting with rotating updrafts on the left and right flank of a mature cell. In an ambient flow with unidirectional **forward** shear the rotation is cyclonic on the

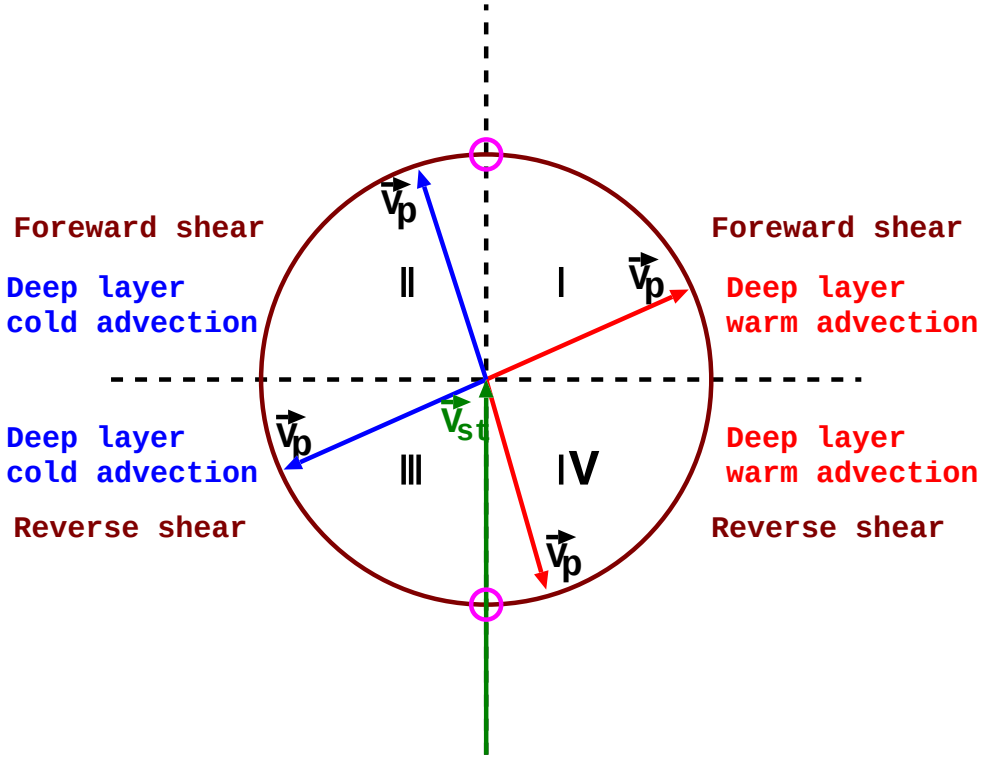

Figure 13: Schematic representation of the influence of deep layer temperature advection and vertical wind shear on the movement of multicell DMC. $\vec{V}_{st}$ is the steering level wind, $\vec{V}_p$ the propagation velocity determined by the preferred region of new cell formation and $\vec{V}_{st} + \vec{V}_p$ the velocity of the DMC system.

right flank and anticyclonic on the left flank.(e.g. Nielsen, 2006). In a **reverse** shear case the rotation is opposite with anticyclonic and cyclonic rotation on the right and left flank of the mature cell, respectively.

7.2 The influence of non-unidirectional vertical wind shear on development of multicell DMC

Cases with unidirectional shear are not so common in the atmosphere. Above the PBL the geostrophic wind, which is a good approximation for large-scale flow in the extratropics, has unidirectional vertical shear only if the horizontal Temperature Advection (TA) is zero. With non-zero TA the development and motion of multicell DMC's deviates from the results described in section 6. In the latter section $\vec{V}_p = (u_p, 0)$, where u_p is the propagation velocity parallel to $\vec{V}_{st}$. If TA is non-zero (either warm or cold advection) the flow also has vertical wind shear along the direction perpendicular to $\vec{V}_{st}$, which in general means that $\vec{V}_p = (u_p, v_p)$ and $v_p \neq 0$. The impact of TA on $\vec{V}_p$ is shown schematically in Figure 13. In this figure the circle shows for a constant $\vec{V}_{st}$ the position of the arrow head of $\vec{V}_{st} + \vec{V}_p$ with varying TA. The circle, shown in Figure 13, is divided into four sectors, labelled I, II, III and IV. Sector I represents warm advection ($TA > 0$) in **forward** shear, sector II cold advection ($TA < 0$) in **forward** shear, sector III cold advection in **reverse** shear and sector IV warm advection in **reverse** shear.

In **forward** shear the system motion is slower than in unidirectional shear, but still faster than the motion of individual cells. The unidirectional shear case in **forward** shear is where $v_p = 0$ and $u_p = |\vec{V}_p|$ (in Figure 12 where $\vec{V}_p + \vec{V}_{st}$ points to the small circle at the top of the larger circle).

In **reverse** shear the system motion is faster than in unidirectional shear, but still slower than the

Figure 14: Transport of moisture from the troposphere to the lower stratosphere by an overshooting top in a rapidly growing convective cell. The overshooting top in the stratosphere is illuminated by lightning. Photo by Borja Santiago.

motion of individual cells. The unidirectional shear case in **reverse** shear is where $v_p = 0$ and $u_p = -|\vec{V}_p|$ (in Figure 13, where $\vec{V}_p + \vec{V}_{st}$ points to the small circle at the bottom of the larger circle). In moderate shear $\vec{V}_p$ is primarily determined by LPP. In warm/cold advection LPP generates upward acceleration to the right/left of the where new cells, in absence of factors like gradients in CAPE and CIN, most likely forms where lifting of air at outflow boundaries from mature cells is largest. Like forcing by LPP the outflow boundary forcing in warm/cold advection tends to be strongest to the right/left of $\vec{V}_{st}$, where the near-surface wind perpendicular to $\vec{V}_{st}$ is in the opposite direction of the outflow.

In strong shear the left/right moving supercell generated by NLPP is suppressed by LPP in warm/cold advection, resulting in a right moving supercell storm in warm advection and a left moving supercell storm in cold advection.

7.3 Other factors contributing to cloud burst/flash-flood

The vertical wind shear is clearly an important factor contributing to self organisation of DMC, but other factors can also play important roles. If for example DMC is initiated in a region with significant horizontal gradients in CAPE and CIN their effect on new cell formation can in some cases overrule the wind shear effect, in particular if the latter is weak. Consider Figure 11a and add a CAPE gradient in the opposite direction of $\vec{V}_{st}$ and a CIN gradient in the direction of $\vec{V}_{st}$. This kills formation of new cells in front of the mature cell and favours formation of new cells on its rear side, forming a backward building multicell system like in the reverse shear cases in Figure 11b. Significant gradients in CAPE and CIN are sometimes present along coast lines and may change sign depending on variations in solar insolation. Large gradients in CAPE and CIN are usually also present across frontal zones.

Cell development in nearly stationary surface convergence lines may also give rise to cloud bursts/flash-floods if the steering wind is parallel to the convergence line.

Longer lasting lifting of potential unstable air over steep orography can also give rise to cloud burst/flash-flood.

References

Bluestein, H.B., 1993. Synoptic-Dynamic Meteorology in Midlatitudes. Volume 2. Observations and Theory of Weather Systems. Oxford University Press, Chp. 3, 447-448.

Duncan, C.N.,1978. Baroclinic instability in a reversed shear flow. Meteorol. Mag.,107,17-23.

Klemp, J.B., 1987. Dynamics of tornadic thunderstorms. Ann. Rev. Fluid. Mech., 19, 369-402.

Markowski, P. and Y. Richardson, 2010. Mesoscale Meteorology in Midlatitudes. Wiley-Blackwell.

Nielsen, N.W.,and C. Petersen, 2003. A generalized thunderstorm index developed for DMI-HIRLAM. DMI Scientific Report 03-16, available at www.dmi.dk/laer-om/generelt/dmi-publikationer/videnskabelige-rapporter.

Nielsen, N.W.,2006. A short introduction to the dynamics of severe convection. DMI Scientific Report 06-02, available at www.dmi.dk/laer-om/generelt/dmi-publikationer/videnskabelige-rapporter.